Piezoresistive Pressure Sensor Array for Robotic Skin

Fahad Mirza [a], Ritvij R. Sahasrabuddhe[a], Joshua R. Baptist[b], Muthu B. J. Wijesundara[a], Woo H. Lee[a], *Dan O. Popa[b]

[a]University of Texas at Arlington Research Institute, 7300 Jack Newell Blvd., S., Fort Worth, TX, 76118, USA
[b]NGS Lab. Dept. of Electrical and Computer Engineering, University of Louisville, Louisville, KY, 40292, USA

ABSTRACT

Robots are starting to transition from the confines of the manufacturing floor to homes, schools, hospitals, and highly dynamic environments. As, a result, it is impossible to foresee all the probable operational situations of robots, and pre-program the robot behavior in those situations. Among human-robot interaction technologies, haptic communication is an intuitive physical interaction method that can help define operational behaviors for robots cooperating with humans. Multi-modal robotic skin with distributed sensors can help robots increase perception capabilities of their surrounding environments.

Electro-Hydro-Dynamic (EHD) printing is a flexible multi-modal sensor fabrication method because of its direct printing capability of a wide range of materials onto substrates with non-uniform topographies. In past work we designed interdigitated comb electrodes as a sensing element and printed piezoresistive strain sensors using customized EHD printable PEDOT:PSS based inks. We formulated a PEDOT:PSS derivative ink, by mixing PEDOT:PSS and DMSO. Bending induced characterization tests of prototyped sensors showed high sensitivity and sufficient stability.

In this paper, we describe SkinCells, robot skin sensor arrays integrated with electronic modules. 4x4 EHD-printed arrays of strain sensors was packaged onto Kapton sheets and silicone encapsulant and interconnected to a custom electronic module that consists of a microcontroller, Wheatstone bridge with adjustable digital potentiometer, multiplexer, and serial communication unit. Thus, SkinCell's electronics can be used for signal acquisition, conditioning, and networking between sensor modules. Several SkinCells were loaded with controlled pressure, temperature and humidity testing apparatuses, and testing results are reported in this paper.

Keywords: Robot skin sensor arrays, piezoresistive strain sensors, Electro-Hydro-Dynamic printing, EHD, PEDOT:PSS, piezoresistive sensor array, inkjet printing.

1. INTRODUCTION

For the last 30 years, researchers have been studying skins for robots similar to human beings that can sense temperature and pressure. It has been reported that the robot's ability to detect exterior forces can improve the communication with humans and the environment, increase the safety and facilitate the human guided behavior learning [1][2]. This research will one-day lead to a robust and dependable human-robot interaction that is adaptable to both different users and tasks. It will expedite the research on social robotics and physical human robot interaction (pHRI).

Like human skin, robot skin can have various sensing modalities e.g. pressure, temperature, vibration, proximity etc. Integrating different types of sensors is difficult for conventional semiconductor manufacturing process because of different sensor materials, different process parameters they require, and the 3D topographical nature of skin. In addition, conventional semiconductor manufacturing has limitations with production on large, uneven and flexible substrates. Flexible substrates are needed because the robot itself has numerous curved shapes. 3D printing is an additive

* Dan Popa; dan.popa@louisville.edu; phone: 502-852-1410; http://www.ngs.louisville.edu

manufacturing technique that has been proposed to manufacture robotic skin sensors. The spatial resolution of the sensors needs to be high enough for safe interaction. However, data acquisition rates will be affected (slowed) considerably by increasing spatial resolution. Fabrication challenges, including signal routing and packaging also increase as we attempt to miniaturize skin sensors. Thus, developing sensor fabrication and data acquisition methods that are scalable and can be applied to an appropriate pHRI scenario are important challenges to overcome.

Once sensor skin fabrication and interfacing is completed, sensor performance must also be evaluated. Performance includes sensor response to temperature changes, asking questions such as does the output response drift over time etc. Challenges include developing efficient, controlled and automated methodologies to characterize these sensors. Finally, the sensor performance must be evaluated in conjunction with the robot's control system. For instance, experiments must be conducted to characterize how pressure sensing capabilities are helping cooperative robots (coRobot) during pHRI.

The paper presents several aspects of robot skin manufacturing and characterization. Electro-Hydro-Dynamic (EHD) technology was used to print pressure sensors on flexible substrates. The printing procedure and quality depends on several parameters, such as applied voltage, applied pressure, nozzle distance from substrate, speed of printing etc. Different combination of the parameters was used to print and then compared under the microscope to check the quality of printing in terms of how evenly the ink spreads to optimize the EHD printing process. LabVIEW based automated control software was developed to implement the automation of printing and calibration, replacing previous manual steps and to provide higher throughput. An automated force controlled setup was used to characterize 4x4 pressure sensor arrays. In addition, sensitivity according to temperature and humidity changes, and signal to noise ratio were measured.

2. PREVIOUS WORK

Skin for robots have been studied for several decades and must have similar features in order to interact with human environments. Tactile sensing is one of the essential parts among all the sensing capabilities and tactile sensors have been extensively reviewed in [3]. As early as 2001, Lumelsky et al. [4] showed how robots can be benefited with IR sensors to interact with a human in an unstructured environment. Much of the supporting technology, such as manufacturing of flexible PCB or robots with multi-sensing modules has appeared since this pioneering work. They also demonstrated a ballerina danced with a sensorized robot arm without colliding with it, which can detect nearby object or human by using infrared sensing taxels.

A leading research group from Germany developed HEX-O-SKIN, a self-organizing multimodal sensing modules that can sense temperature, pressure, acceleration and force [5]. They developed their own pressure sensor while integrating other off-the-shelf sensors into modules. Each module has a unique ID and local intelligence to preprocess information, which in turn reduces the message overhead through the network. An accelerometer maps the modules relative position with respect to the robot host, while each module has four ports to communicate with neighboring modules. A highly redundant sensor structure was demonstrated on a KUKA arm and HRP-2 robot.

Another team from Italy developed Roboskin [6], which consists of twelve capacitive pressure sensing taxels, among which two of them are used to compensate temperature drifting for other ten taxels. Each sensor module is made of a flexible triangular shape PCB so that it can be placed on any part of a robot. The module also contains an off-the-shelf analog-to-digital converter, and thirteen modules are connected with each other via I^2C bus. The Roboskin was tested on iCub, Kasper and Nao robots.

An MEMS barometer chip based TakkTile [7] is a low cost tactile sensor array that has all the necessary circuitry on a small PCB with a sensitivity of 1 gram. It has a built-in ADC and I^2C communication chip. The MEMS barometer chip on PCB is casted under rubber that enhances the sensitivity and consistency.

Conventional semiconductor integrated circuit technology uses rigid substrates, such as silicon wafers that are not suitable for robot skin. Robot skin requires conformal and flexible sensors that can be stretchable and bendable to adapt to various shapes on robot links. Research has been recently conducted towards sensor fabrication on flexible substrates. A group from Princeton University developed elastomeric skin where sub-circuits are interconnected by stretchable metallization [8] on a flexible substrate. Dahiya et al. [9] developed ultra-thin bendable electronic skin that uses 2.5µm silicon wires and microstructures on polyimide. Piezoelectric tactile sensor on a flexible ultra-thin polyimide was developed in [10].

Among various fabrication techniques, lithography has been widely used to fabricate microelectronics and micro-electro-mechanical systems (MEMS). However, lithography is inherently not suitable for structures that have more than two dimensions [11][12].

3. SENSOR FABRICATION

Physical human-robot interaction requires multi-modal sensors, in a form of artificial skin, especially in a dynamically changing environment. It is challenging to integrate multi-modal sensors under one substrate in standard semiconductor manufacturing methods because of 3-D topographies. As a result, some researchers have recently proposed 3D printing technology [12]. Among non-lithographic methods, Electro-Hydro-Dynamic (EHD) ink-jet printing has the potential features for multi-modal sensors with tunable resolution down to 1 micron, supports a wide range of ink materials and can manufacture 3D features on flexible substrates. It is one of the promising additive manufacturing methods that can be used as an alternative.

3.1 EHD Printing

In this paper, a well-known piezoresistive material, PEDOT:PSS, was used as a pressure sensing material using EHD printing. The EHD printing method creates an electric field to dispense fluid out of a nozzle. A high voltage electric field generates well-proportioned jetting, which in turn helps to shrink the smallest features by an order of magnitude below the nozzle size [14]. The combination of pressure and electric field induces ink-jetting onto the substrate.

Figure 1 shows the schematic diagram of EHD printing system. EHD printing supports a wide range of materials, and can print high viscosity materials e.g. up to 1000cP, as opposed to 50cP achievable with conventional inkjet or piezoelectric printing.

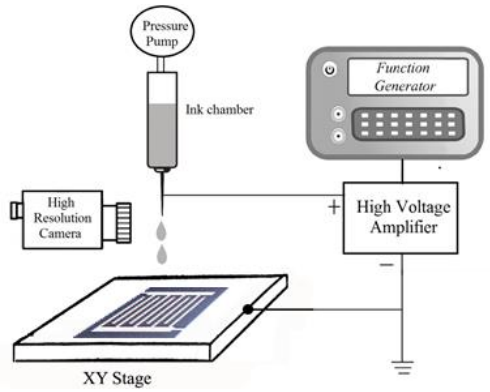

Figure 1. EHD Printing Setup.

Because of the electric field's pulling and focusing feature, this method can provide finer jetting compared to piezo-jet based printing. Furthermore, the electric field generates a stable and continuous flow, which is helpful to print a uniform line over large areas [15][16].

3.2 Piezoresistive Pressure Sensor

Pressure sensors have been used in industry for numerous applications including biomedical, automobiles, space and environment [17]. There are three main types of pressure measurement techniques: piezoresistive, piezoelectric and capacitive, and numerous researches have explored these transducers over the years [18][19]. Capacitive sensors create a variable capacitance to detect strain caused by pressure. These sensors are good for low-pressure measurements. However, because of their inherent parasitic noise, their linearization is poor. Piezoelectric sensors are suitable for dynamic pressures but have poor response for measuring static pressures. Piezoresistive sensors provide variable resistance for applied pressure. They are suitable for static and dynamic response, but are generally sensitive to temperature changes. A wide variety of materials exhibit the piezoresistive effect [20], with high sensitivity and cost effectiveness in manufacturing.

We have selected a piezoresistive sensing material, PEDOT:PSS, to fabricate pressure sensors. PEDOT:PSS is a conductive and transparent polymer that is stretchable, highly ductile and stable. It has been used as smart textiles [21], flexible piezoresistive strain gauge sensors [22][23] and touch sensors [24]. Typical conventional metal films has a gauge factor of 2, PEDOT:PSS's gauge factor ranges from 5 to 20, makes it an ideal choice for our work.

The substrate of our sensor is fabricated by MEMS technology, using lithography, deposition and lift-off to make conductive traces. An interdigitated electrode (IDE) structure with micron-scale features on a flexible polyimide (Kapton) substrate serves as the substrate on which PEDOT inks are printed. 4x4 sensory array is illustrated in Figure 2. Each taxel is marked to identify an individual taxel. Zero insertion force connector is used to interconnect 16 taxels. The sensor was encased by sandwiched between two RTV silicon rubber (P-10) pads from Silicone Inc. Figure 3 shows the dimensions of a IDE structure.

(a)

(b)

Figure 2. (a) 4x4 sensor array with markings (b) Packaging with P-10 silicone.

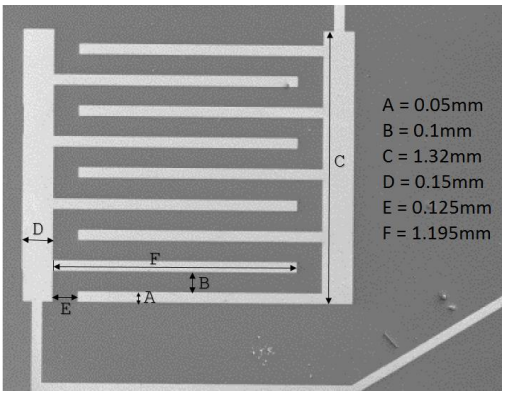

Figure 3. Interdigitated Electrode structure's dimension.

3.3 Ink Formulation and Characterization

Ink was formulated using PEDOT:PSS as a primary material and Dimethyl sulfoxide (DMSO) as solvent. DMSO has a broad collection of miscible organic solvents and has a high melting point. First, high viscosity screen printing PEDOT:PSS paste was dissolved in DMSO to obtain desired ink characteristics including low viscosity and low surface tension. The weight-to-weight composition of PEDOT:PSS and DMSO solvent was 1:3. The masses of each component of the mixture were measured using an Ohaus model EF214C analytical. The primary solvent is first weighed in a

centrifuge tube, along with any other non-colloidal liquids. Solid materials are then added stepwise in ~250mg increments and mixed between each step for 10 seconds with a vortex mixer. In the original vial, the contents are mixed in a rotary tumbler for no less than 5 hours to ensure solids are thoroughly dissolved. After thorough integration of solid materials into the solvent, PEDOT:PSS is added by mass into the solvent mixture. This is done at one time with no intermediate mixing. After the PEDOT:PSS is added, the mixture is re-tumbled for at least 15 hours. Prior to printing, the ink is vortexed then sonicated for 15 minutes.

3.4 Printing Parameter Optimization

There are four printing parameters that need to be investigated: the applied voltage, pressure, nozzle travel speed and distance between nozzle and substrate. Wide ranges of these parameters were used for a Design of Experiments trial to find optimized parameters for each ink. A 32-gauge nozzle is used for printing experiment. Agilent 33220A wave from generator was used to generate 1kHz square wave signals controlling the electric field in order to obtain drop-on-demand ink jetting. A Trek PM04015A Generator/Amplifier was used as high voltage power supply. For pressure control, the Alicat PCV110 pressure pump can generate pressures up to 25kPa. Appropriate parameter finding trials are shown in Table 1.

Table 1. Parameters for printing (PEDOT:PSS) DMSO ink.

Pressure (kPa)	Distance b/w nozzle and substrate (μm)	DC voltage (V)	Speed (mm/min)
0.15	600	1000	50
0.15	700	1000	150
0.25	600	1600	300
0.50	700	1600	500
1	700	1800	50
1	800	1800	50

The sample straight lines were printed on gold plates and were examined under a Digital Microscope, Hirox KH-7700, to compare results both quantitatively and qualitatively. Representative printing samples are shown in Figure 4. For example, the line on the left of Figure 4 is wider and has more PEDOT:PSS compare to the right lines. Based on the visual feedback, we choose 800μm distance between nozzle tip and substrate, 1.8kV, 1kPa pressure with 3mm/s nozzle travel speed.

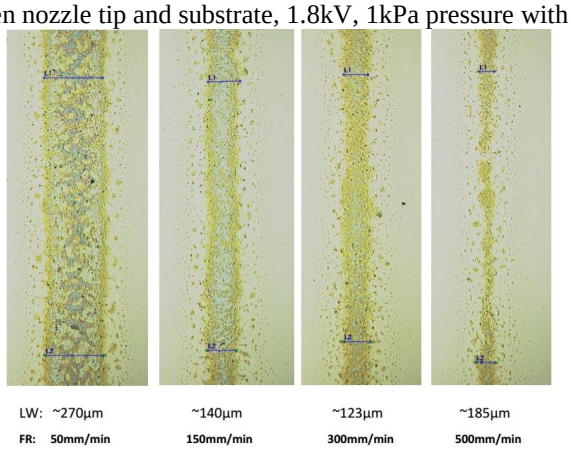

Figure 4. Sample DMSO ink print with 800μm Nozzle Height, 1.8kV, 1kPa.

3.5 Printing Calibration

Previously, substrates were placed below the print nozzle, and had to be manually aligned with the print head axes, which in turn made the printing process time consuming [26]. In order to speed up the printing process, a kinematics identification technique was adapted from [25] in order to map the sensor's local coordinate system with respect to global a coordinate system of the print head XYZ stages. As a result, the initial orientation of the substrate can be corrected via a few

experiments. After this calibration scheme, an open loop controller is precise enough to control the XYZ motorized stages over large distances.

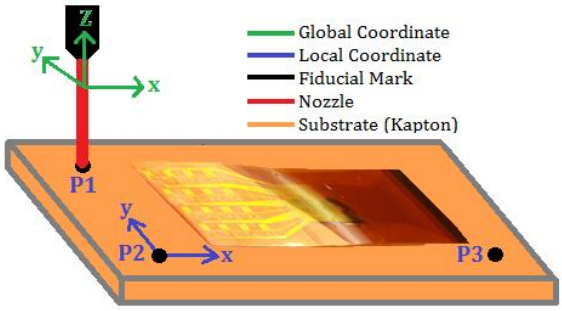

Figure 5. Local and Global Coordinate Frames.

The calibration method requires three fiducial marks on the local coordinate system on the sensor (P_1, P_2, P_3 in Figure 5). The system records those marks in the global coordinate value using encoder values of XYZ stages. After that, global coordinate values to attain a local coordinate point (p, q) can be calculated by equations (1) and (2) [25]:

$$R = R_1 + (R_2 - R_1)\left(\frac{p - p_1}{p_2 - p_1}\right) + \left(R_3 - \hat{R}\right)\left(\frac{q - q_1}{q_3 - q_1}\right) \quad (1)$$

$$\hat{R} = R_1 + (R_2 - R_1)\left(\frac{p_3 - p_1}{p_2 - p_1}\right) \quad (2)$$

where, (p_1, q1), (p_2, q2), (p_3, q3) are local coordinates of P_1, P_2 and P_3 fiducials respectively (i.e. on the sensor substrate), P is an arbitrary point with local coordinates of (p, q) (i.e. any point of interest on the sensor substrate), R_1, R_2 and R_3 are the global coordinate values of the XYZ stage of P_1, P_2 and P_3 respectively with nozzle pointing to that location, and R represents the global coordinates of the nozzle to point at P.

The values of P_1, P_2 and P_3 can be obtained directly from the design layout, whereas R_1, R_2 and R_3 values are read from the encoder on the print head stages. The reference points are obtained by placing the nozzle on those fiducial points. The process is observed through a 5x lens CCD camera that provides 3.2µm/pixel image resolution.

The XYZ print head positioning system is controlled by Aerotech A3200 Direct Drive Stage System. The system can control up to 32 axes and supports two communication interfaces, EitherCAT and Profinet. The servo resolution in any axis is as precise as 1µm, which is adequate for EHD printing.

A program written in LabVIEW was used to automate the calibration process and resulting trajectories. After calibration, a user interface accepts fiducial local and global coordinates as input. Once the calibration is done, the program loads a set of local coordinates in the form of a text file, and generates XYZ print head position to follow a printing trajectory. A printing path parallel to the direction of the IDE comb was chosen in our experiments as shown in Figure 6. The program then generates an array of stage encoder values defining trajectory via points. In order to have a continuous motion from one point to another, the distance between two points is calculated and normalized for all the axes and then multiplied that with the desired joint velocity, which in our case was 3mm/s.

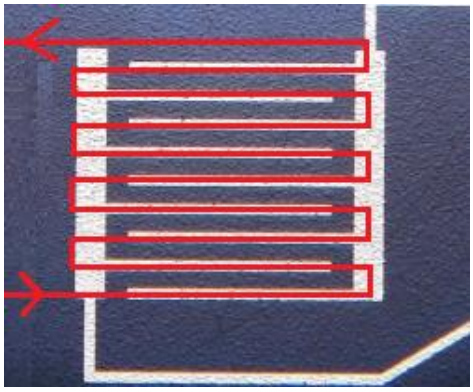

Figure 6. Sensor printing trajectory.

3.6 SkinCell: Sensor Array Electronics Module

A sensor array SkinCell was interfaced to service 16 single interdigitated structures in a 4-by-4 arrangements. Instead of impractically building 16 identical signal conditioners for single sensors, we added an analog multiplexer, CD74HC4067 that can switch between 16 sensors and connect those with the Wheatstone bridge one at a time. Furthermore, as different interdigitated structures have different resistance value, we used a digital potentiometer, AD5174, to balance out the bridge by tuning individual taxel resistances. It is a 10kΩ potentiometer with 1024 position and can be configured by SPI communication protocol.

The data acquisition system for the entire 4x4 SkinCell was controlled from an IC, ATmega2560, an 8-bit RISC based microcontroller manufactured by ATMEL. It is a high-performance, low power system with 86 general purpose I/O pins, 4 USARTs and 10-bit A/D converter. It can achieve a throughput of 16 MIPS.

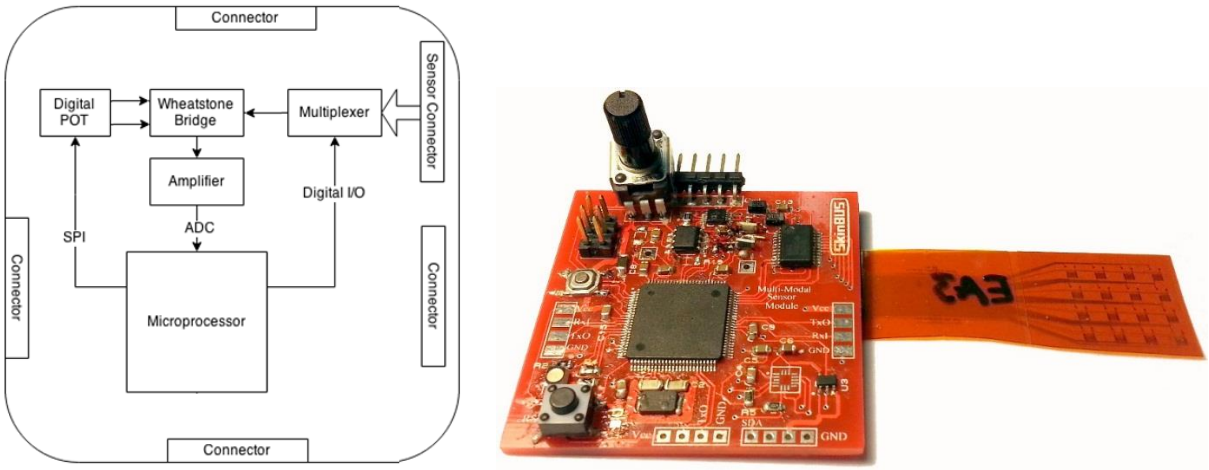

(a) (b)

Figure 7. SkinCell: (a) block diagram and (b) SkinCell connected with 4x4 sensory array.

The block diagram of the SkinCell is shown in Figure 7 (a). The digital potentiometer was configured through the SPI bus, while the output of the instrumentation amplifier is connected with an ADC channel. In order to provide a scalable design for large area robot skins, the SkinCell was designed to communicate with neighboring SkinCells through USART, which is placed on the four sides of the board. The resulting printed circuit board of a SkinCell has dimension of 48mm by 50mm as shown in Figure 7 (b).

4. EXPERIMENTAL RESULTS

Testing a piezoresistive pressure sensor requires a set of high end equipment that has high resolution analog-to-digital converter, susceptible to noise and can collect data in real time. The system consists of National Instruments real-time FPGA hardware, compact RIO (cRIO), and controlled by the software package, LabVIEW. cRIO has a 400MHz processor and 8 slots for swappable devices.

Two different sets of setup were used to test the sensors. As shown in Figure 8, a plunger vertically attached to the Newport linear stage was used to load the pressure sensor under controlled force conditions. The radius of a tip is 3.2mm. The motion and force controller of the pressure testing hardware is thoroughly described in [26, 27]. In the second setup an off-the shelf temperature and humidity sensor, HTU21D, from Measurement Specialties, was used to log the temperature and humidity change. A cardboard box was used to cover the HTU21D and a sensor array. Then the temperature of the environment was varied by an external heat source. Although the temperature and pressure sensors location was not identical, the close proximity and the small volume of the cardboard box made it likely that they experienced close temperature variations. Humidity was varied by applying water vapor.

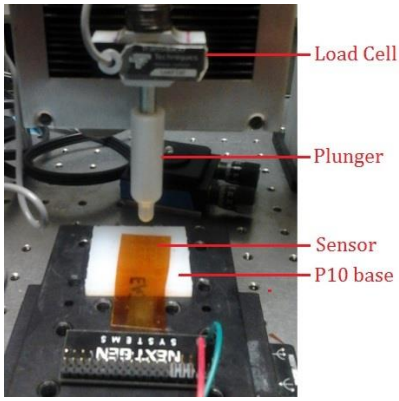

Figure 8. Experimental Setup.

4.1 Sensitivity according to temperature and humidity variations

Environmental test was performed to evaluate the sensitivity according to temperature and humidity changes. We conducted temperature cycling tests for Skin Cells and individual sensors to investigate their sensitivity. The sensor environment started at room temperature, 24^0C, and was heat up to around 40^0C and then cooled down to around 10^0C and came back to the room temperature again. Test was conducted on 28 IDE structures for three times. Table 2 tabulates sensitivity for 12 tests and its average sensitivity was 175 mV/^{0}C.

Table 2. Temperature Sensitivity.

Test No.	Resistance in room temperature (Ω)	Sensitivity,α (mV/^{0}C)	Average Sensitivity (mV/^{0}C)
1	345	190	175
2	212	170	
3	250	176	
4	301	150	
5	313	180	
6	225	175	
7	311	183	
8	330	181	
9	280	176	
10	202	140	
11	323	191	
12	295	182	

Humidity test was conducted on 28 IDE structures for three times. Table 3 tabulates test results, and its average sensitivity was 7.88 mV/%RH.

Table 3. Humidity Sensitivity.

Test No.	Resistance in room temperature (Ω)	Sensitivity,α (mV/%RH)	Average Sensitivity (mV/%RH)
1	345	8.54	7.88
2	212	7.89	
3	250	7.56	
4	301	8.02	
5	313	8.12	
6	225	7.6	
7	311	8.3	
8	330	8.4	
9	280	7.68	
10	202	6.89	
11	323	7.8	
12	295	7.81	

4.2 Repeatability

Repeatability test with a constant applied pressure was performed to evaluate how repeatable the sensor is. The experiment was conducted on taxels #1, #6, #11, and #16 to have both interior and edge effects as illustrated in Figure 5. 1lb pressure was applied and repeated for 10 times for each taxel. With each trial the responses were averaged over time. Between measurements, the plunger was off the sensor. P-10 silicone rubber was used under the sensor, but nothing was placed on top of the sensor in order to avoid additional non-linearity. The sensor and electronics were warmed up for 60 minutes to avoid any temporal thermal drift. Repeatability test results are shown in Figure 9.

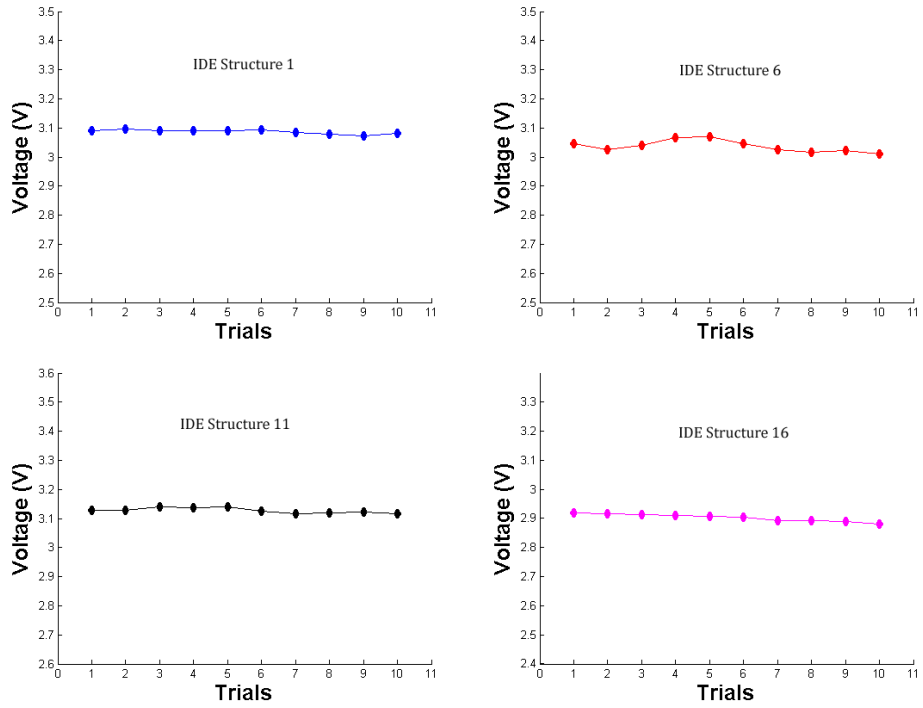

Figure 9. Repeatability test results. Taxels #1, #6, #11, #16.

Table 4 depicts the resulting performance of loading the plunger on top of taxels #1, #6, #11, #16 respectively.

Table 4. Sensor Repeatability.

Taxel #	Avg. Applied Pressure (lb)	Avg. Output (V)	Std. Dev. (mV)
1	1.062	3.086	7.1
6	1.043	3.037	20.7
11	1.057	3.127	12.9
16	1.049	2.902	9.0

The sensor array exhibits repeatable results with an average standard deviation of 12.4mV across different structures. The result shows that loading taxels #1 and #16 have smaller standard deviation than taxels #6 and #11. This can be explained by them being closer to the edge of the sensor, thus experiencing more strain.

4.3 Signal to Noise Ratio

Noise is an inseparable issue when it comes to real world signals. There are various standard ways that show how much a signal is affected by noise. Signal-to-Noise Ratio (SNR) provides an idea how strong a signal is compared to unwanted noise. It is defined as:

$$SNR = \frac{\mu_P - \mu_R}{\sigma} \quad (3)$$

where, μ_P is mean value when pressure is applied, μ_R is mean value in resting position, σ is standard deviation of the signal [28].

An example of SNR calculation is shown in Figure 10 across structure 16. μ_P and μ_R were choose as a little less and a little more, respectively, to make sure it covers all the averaged values. Standard deviation was calculated from the resting position noise. 1lb pressure was applied and hold it for 10 seconds. In between measurements, the tip was off the sensor. The procedure was repeated 10 times.

Table 5. SNR of sensor.

Taxel #	Std. Dev.	SNR
1	1.7844	13.07
6	2.6144	17.01
11	2.02	16.92
16	2.1376	20.6

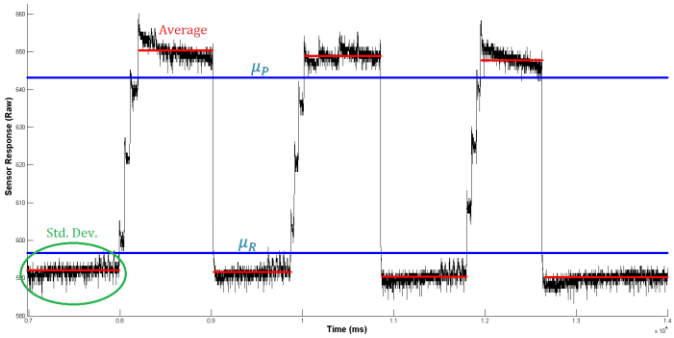

Figure 10. Structure 16 SNR calculation.

The results shown in Table 5 provides insight into the amount of SNR expected from the sensor array. Taxel #1 is the farthest structure from the connecting pad, hence affected most by the noise while taxel #16 is the nearest structure and hence less affected by noise.

4.4 Cross talk between taxels

The structures on the sensors are close each other. This test exhibits if there us crosstalk between adjacent structures when pressure is applied on a particular structure. The result illustrates that the diagonal structures have negligible crosstalk but crosstalk shows up in four orthogonal structures. While the resistance of the structure, where pressure is applied, decreases because of inward deformation, resistance of adjacent structures increases because of outward deformation. Table 6 tabulates cross talk from adjacent taxels. The unloaded output of the IDE structure was 3V.

Table 6. Crosstalk between taxels.

Center taxel #7 reading (V)	Crosstalk reading from adjacent taxel (V)				Average (V)	Percentage
	#3	#6	#8	#11		
3.13	2.92	2.92	2.93	2.93	2.924	6.76%
3.1	2.89	2.89	2.901	2.91	2.899	6.58%
3.03	2.9	2.87	2.902	2.904	2.9	4.2%

5. CONCLUSIONS AND FUTURE WORK

This paper presented several aspects of robot skin sensor manufacturing and experimental characterization. A 4x4 sensor array was fabricated using EHD printing, packaged, interfaced with electronics (SkinCell) and tested. The advantage of this approach is in flexibility in terms of substrate topography, ink formulation and sensor pitches. Results of sensor printing with PEDOT:PSS mixed with DMSO (1:3) show good crosstalk, SNR, repeatable results across the array, and low sensitivity to humidity. The measured pressure resolution was approximately 0.15 psi for a range of 10psi, and a bandwidth of at least 10 Hz, making them excellent choices for physical human-robot interaction applications. Results also show high temperature sensitivity, therefore in future work we will need to compensate this effect either by monitoring the temperature of the ambient environment using a temperature sensor or by using two strain gauges on the Wheatstone bridge. More printed arrays samples need to be tested and several derivative inks of PEDOT:PSS should be experimentally evaluated [29]. The effect of ink selection, geometrical parameters, and larger skin surfaces on the sensor performance will be investigated in conjunction with the robot control system.

6. ACKNOWLEDGMENTS

This work was supported in part by the National Science Foundation NRI Grant #IIS-1208623. We wish to thank Ruoshi Zhang and the UTA Research Institute staff for their help with the experimental work and presented in this paper.

REFERENCES

[1] J. Rajruangrabin and D. O. Popa, “Enhancement of Manipulator Interactivity through Compliant Skin and Extended Kalman Filtering,” in *IEEE Int. Conf. on Automation Science and Engineering*, 2007, pp. 1111–1116.

[2] B. D. Argall and A. G. Billard, “A survey of Tactile Human-Robot Interactions,” *Robotics and Autonomous Systems*, vol. 58, no. 10, pp. 1159–1176, 2010.

[3] M. Cutkosky, R. Howe and W. Provancher, "Ch. 9: Force and Tactile Sensors," in Springer Handbook of Robotics, Springer Handbooks, 2008.

[4] V. J. Lumelsky, M. S. Shur and S. Wagner, “Sensitive Skin,” in IEEE Sensors, vol. 1, pp. 41-51, 2001.

[5] P. Mittendorfer and G. Cheng, "From a Multi-Modal Intelligent Cell to a Self-Organizing Robotic-Skin," in ICRA 2013, 2013.

[6] Cannata, G., Maggiali, M., Metta, G. and Sandini, G., An embedded artificial skin for humanoid robots. In Multisensor Fusion and Integration for Intelligent Systems, 2008, IEEE Int. Conference on (pp. 434-438).

[7] Y. Tenzer, L. P. Jentoft and R. D. Howe, "Inexpensive and Easily Customized Tactile Array Sensors using MEMS Barometers Chips," Harvard School of Engineering and Applied Sciences, 2012.

[8] S. Wagner, S. P. Lacour, J. Jones, I. H. Pai-hui, J. C. Sturm, T. Li and Z. Suo, "Electronic skin: architecture and components," Physica E: Lowdimensional Systems and Nanostructures, vol. 25, no. 2, pp. 326-334,2004.

[9] R. S. Dahiya, G. Metta, M. Valle and G. Sandini, "Tactile sensing—from humans to humanoids, " *IEEE Transactions on Robotics*, vol. 26, no. 1, pp. 1-20, 2010.

[10] L. Maiolo, A. Pecora, F. Maita, A. Minotti, G. Fortunato, D. Ricci and G. Metta, "Enhanced Piezoelectric Hybrid Tactile Sensors Fully Integrated on Ultra-Thin Polyimide Substrates for Robotic Applications," in ICRA 2013: Research Frontiers in Electronic Skin Technology, Karlsruhe, Germany, 2013.

[11] K.-H. Choi, A. Khan, H.-C. Kim, K. Rahman, K.-R. Kwon, N. M. Muhammad and Y. H. Doh, Electrohydrodynamic inkjet-micro pattern fabrication for printed electronics applications, INTECH Open Access Publisher, 2011.

[12] "Ceramics - Research." Princeton University," [Online]. Available: http://www.princeton.edu/~cml/html/research/ehdp.html.

[13] "ijetae," [Online]. Available: http://www.ijetae.com/files/Volume4Issue5/.

[14] Chen, C.-H., Saville, D. A., and Aksay, I. A., "Scaling laws for pulsed electro-hydro-dynamic drop formation," Applied Physics Letters 89, 12410, 2006.

[15] Lee, D.-Y., Lee, J.-C., Shin, Y.-S., Park, S.-E., Yu, T.-U., Kim, Y.-J. and Hwang, J., "Structuring of conductive silver line by electrohydrodynamic jet printing and its electrical characterization," *Journal of Physics: Conference Series.* Vol. 142. No. 1. IOP Publishing, 2008.

[16] Sidhu, R., Sin, J., Lee, W. H., Stephanou, H. E., and Wijesundara, M.B.J., "Electrohydrodynamic printing of metal oxide microstructures," *International Conference On Micromanufacturing*, pp. 458-461, 2012.

[17] Chatzandroulis, S.; Goustouridis, D.; Normand, P.; Tsoukalas, D. "A solid-state pressure-sensing microsystem for biomedical applications". *Sens. Actuators A Phys.* 1997, *62*, 551–555.

[18] Eaton, W.P.; Smith, J.H. "Micromachined pressure sensors: Review and recent developments," *Smart Mater. Struct.* 1997, *6*, 530–539.

[19] Barlian, A.A.; Park, W.T.; Mallon, J.R., Jr; Rastegar, A.J.; Pruitt, B.L. "Review: Semiconductor piezoresistance for microsystems," *IEEE Proc.* 2009, *97*, 513–552.

[20] Chiolerio, A.; Roppolo, I.; Sangermano, M. "Radical diffusion engineering: Tailored nanocomposite materials for piezoresistive inkjet printed strain measurement," *RSC Adv.* 2013, *3*, 3446–3452.

[21] Calvert, P., Patra, P., Lo, T-C., Chen, C., Sawhney, A., and Agrawal, A., "Piezoresistive sensors for smart textiles," Proc. SPIE 6524, *Electroactive Polymer Actuators and Devices*, (2007).

[22] Latessa, G., Brunetti, F., Reale, A., Saggio, G., and Carlo, A. D., "Piezoresistive behavior of flexible PEDOT:PSS based sensors," *Sensors and Actuators B: Chemical*, 139 (2), 304-309 (2009).

[23] Lang, U., Rust, P., and Dual, J., "Towards fully polymeric MEMS: Fabrication and testing of PEDOT/PSS strain gauges," *Proc. Micro- and Nano-Engineering*, 1050-1053 (2007).

[24] Takamatsu, S. and Itoh, T., "Novel MEMS Devices Based on Conductive Polymers," *Electrochemical Society, Interface*, (2012).

[25] Das, A.N.; Zhang, P.; Lee, W.H.; Popa, D.; Stephanou, H., "μ^3: Multiscale, Deterministic MicroNano Assembly System for Construction of On-Wafer Microrobots," *IEEE International Conference on Robotics and Automation*, 2007, Volume-Issue 10-14, Page(s):461 – 466, Roma, Italy, April 2007.

[26] Sahasrabuddhe, R., *Development, Testing and Characterization of Electronic Skins for Robots*, M.Sc. Thesis, University of Texas at Arlington, Department of Electrical Engineering, December 2015.

[27] Shook, K.; Ahsan, H.; Lee, W.; Popa, D, "Experimental Testbed for Robot Skin Characterization and Interaction Control" Proc. SPIE 9116, Next-Generation Robots and Systems, June 2014.

[28] "Noise and Noise Rejection." Purdue University, [Online]. Available:https://engineering.purdue.edu/ME365/Textbook/chapter11.pdf

[29] Nothnagle, Caleb, et al. "EHD Printing of PEDOT: PSS Inks for fabricating pressure and strain sensor arrays on flexible substrates." *Proc. of SPIE Vol*. Vol. 9494. 2015.